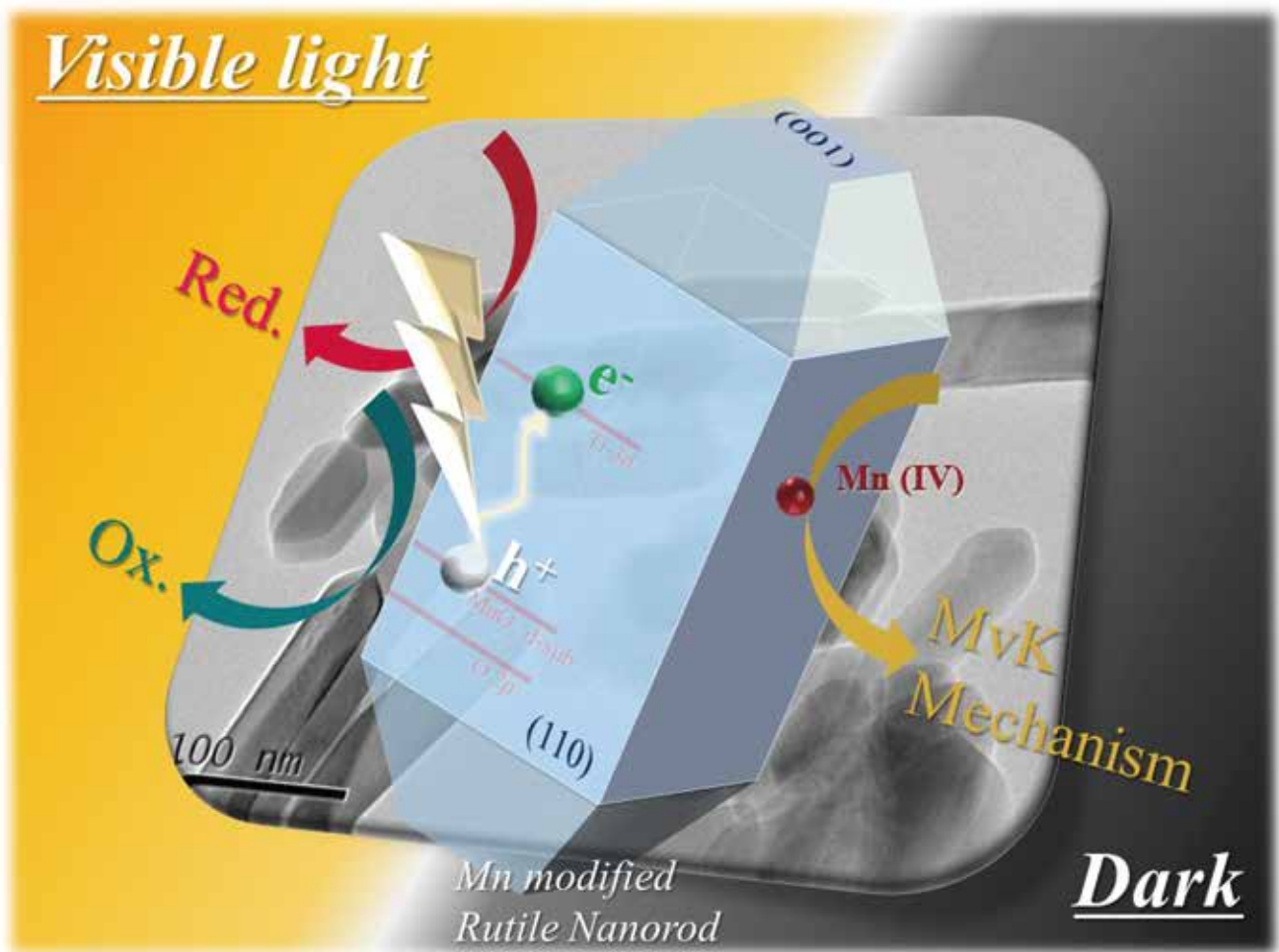


JCS-Japan

October
vol.126



Journal of the Ceramic Society of Japan

2018

FULL PAPER

Crystal face dependence of the decomposition of 2-naphthol in water under dark condition by rutile modified with MnO_x

Mimori SHIOHARA¹, Toshihiro ISOBE¹, Sachiko MATSUSHITA¹ and Akira NAKAJIMA^{1,†}¹Department of Materials Science and Engineering, School of Materials and Chemical Technology, Tokyo Institute of Technology, 2-12-1 O-okayama, Meguro-ku, Tokyo 152-8552, Japan

Crystal face dependence of the decomposition activity of MnO_x -modified rutile-type TiO_2 on 2-naphthol in water in the dark was investigated. Clusters of MnO_x were modified onto (110) and (001) surfaces of rutile single crystals using chemisorption calcination cycle (CCC) processing. The major valences of Mn on (110) were Mn(III) and Mn(IV), whereas those on (001) were Mn(II) and Mn(III). Energy calculations for the MnO_x cluster on (110) corresponded to experimentally obtained results. Rutile nanorods with high (110) ratio were prepared using hydrothermal methods. Under the same conditions, MnO_x was impregnated on the surface using CCC processing. Despite smaller specific surface area and surface Mn concentration, the synthesized nanorod powder on 2-naphthol in water in the dark exhibited almost identical decomposition activity to that of a commercial rutile powder. The ratio of Mn(IV) of the nanorod powder was higher than that of the commercial rutile powder. The normalized activity for the nanorod powder was more than twice as much as that for commercial rutile powder. These results imply that the interface design between the base material and MnO_x clusters plays an important role in the decomposition activity of organic substances in the dark.

©2018 The Ceramic Society of Japan. All rights reserved.

Key-words : Dark, Decomposition, Mn, Rutile, Crystal face

[Received April 9, 2018; Accepted May 31, 2018]

1. Introduction

When ultraviolet (UV) light is illuminated on titanium dioxide (TiO_2), a well-known semiconductor photocatalyst, electron and hole pairs are generated.¹⁾ The electron and hole pairs respectively reduce and oxidize adsorbates on the surface, thereby producing radical species that can decompose most organic compounds and bacteria. Numerous studies have investigated this material for its application to environmental purification.^{2)–6)} Because of its band-gap (3.2 eV for anatase, 3.0 eV for rutile), photocatalytic reaction by pure TiO_2 requires illuminating light that has sufficiently short wavelength for electron excitation, which is in the UV range and which constitutes only a small fraction of the sunlight. Combining the materials with decomposition activity against organic substances in the dark with TiO_2 enables continuous environmental purification.

Recent investigations have revealed that manganese-based oxides (MnO_x) decompose organic compounds under ordinary pressure at the temperatures less than 100°C.^{7)–11)} Their decomposition activity (oxidation) is attributed to the Mars – van Krevelen (MvK) mechanism.^{7)–9)} Very recently, we modified MnO_x onto TiO_2

surface by chemisorption calcination cycle (CCC) processing.¹²⁾ The decomposition activities of the materials on 2-naphthol were evaluated in water at 50°C with and without visible light illumination. Both the decomposition activity in the dark and visible light photocatalytic activity were provided to TiO_2 by the modification of MnO_x . Results demonstrated that the dark activity was provided by the MvK mechanism. Moreover, synergistic effects on decomposition in the dark were inferred for the combination of MnO_x and CeO_y . Decomposition activity in the dark decreased via repeated use. However it recovered by UV illumination or subsequent heating in ambient air.¹³⁾

Further investigation revealed that effects of MnO_x modification on dark activity are less remarkable for anatase-type TiO_2 than for rutile-type TiO_2 .¹³⁾ The major valences of Mn in MnO_x on rutile were Mn(IV) and Mn(III), whereas those on anatase were Mn(III) and Mn(II). Actually, Mn(IV) can be reduced through Mn(III) to Mn(II). Therefore, the high concentration ratio of Mn(IV) in MnO_x implies a large amount of oxidation capability against organic compounds. A plausible explanation of the Mn valence difference between rutile and anatase is interaction with MnO_x . Zhang et al. impregnated MnO_2 onto various carbon materials and investigated the reduction temperature of MnO_2 using H_2 -TPR.¹⁴⁾ They demonstrated that the reduction temperatures for both $\text{Mn(IV)} \Rightarrow \text{Mn(III)}$ and $\text{Mn(III)} \Rightarrow \text{Mn(II)}$ depend on the base material impregnated with MnO_2 . Because MnO_2

† Corresponding author: A. Nakajima; E-mail: anakajim@ceram.titech.ac.jp‡ Preface for this article: DOI <http://doi.org/10.2109/jcersj2.126.P10-1>

possesses a rutile-type crystal structure,¹⁵⁾ the stability of Mn(IV) and activation energy for reduction of MnO_x might be different between anatase and rutile. Based on this consideration, we have improved the decomposition activities in the dark and under visible light by using (Mn, Sn) O_x and SnO_x to control the interaction between rutile and clusters.¹⁶⁾

The interaction between rutile and MnO_x cluster is also expected to depend on the crystal faces of rutile. Earlier comparative studies revealed that photocatalytic activity of the faces with bridging oxygen such as (110) and (100) differs from that of the faces with only in-plane oxygen such as (001).^{17)–21)} For the present study, using the CCC processing and rutile single crystal, we modified (110) and (001) of rutile with MnO_x ; the Mn valence was evaluated. Moreover, rutile nanorod powders with high (110) ratio (elongated to [001]) were prepared and modified with MnO_x . Then the activity of the powders on the decomposition of 2-naphthol in water under dark condition was compared with a commercial rutile powder.

2. Experimental

2.1 Experiment using single crystals

Commercial mirror-polished rutile single crystals of (110) and (001) (Furuuchi Chemical Corp. Ltd., Tokyo Japan) were annealed at 600°C for 1 h in air to remove the residual strain in the surface. This condition was ascertained through preliminary study using X-ray diffraction (XRD, XRD-6100; Shimadzu Corp., Tokyo, Japan). After masking half of the surface, an ethanol solution (8.0 mmol/L) of manganese(III) acetylacetonate [$\text{Mn}(\text{acac})_3$; Wako Pure Chemical Corp. Ltd., Tokyo, Japan] was coated onto the single crystals using spin coating (800 rpm, 50 s + 2500 rpm, 60 s). Then the samples were dried and fired at 500°C for 1 h in air. The microstructure of the coating was evaluated using atomic force microscopy [AFM, JSPM-4200; JEOL, Tokyo, Japan: cantilever NSC36/Ti-Pt (μ -mash)]. The surface chemical composition was measured using an X-ray photoelectron spectroscope (XPS, ESCA 5500MT; PerkinElmer Inc., U.S.A.) with an $\text{AlK}\alpha$ X-ray line (1486.6 eV). The valences of Mn were determined by deconvolution of the Mn2p peak, as they were in earlier studies.^{22)–26)}

2.2 Preparation and characterization of rutile nanorod powders

We prepared rutile nanorod powders using TiCl_4 with reference to previous studies.^{27),28)} A commercial titanium(IV) chloride aqueous solution (TiCl_4 ; Toho Titanium Co. Ltd., Kanagawa, Japan, Concentration: 16–17%) was added (20 mL) to distilled water (50 mL). The solution was stirred at 70°C for 1 day. Then the white precipitate and the remaining solution were placed into the Teflon reactor of a stainless steel autoclave that was heated to 120, 180, or 200°C for 12 or 24 h. It was then allowed to cool. After washing in distilled water, the powder was dried by freeze-drying for 24 h. The obtained powder (1.2 g) was dispersed into an ethanol solution (8.0 mmol/L, 12 mL) of manga-

nese(III) acetylacetonate described above and was stirred for 24 h. After filtration and washing, the powder was dried in vacuum for 24 h. Then it was fired at 500°C for 1 h in air. This impregnation–calcination cycle was repeated three times. For comparison, we also prepared a MnO_x modified rutile sample using a commercial rutile powder (MT150A; Tayca Corp., Osaka, Japan) under the same conditions as those used for our earlier studies.^{13),16)}

The crystalline phase of the powder was evaluated using XRD. Specific surface areas were measured using Brunauer–Emmett–Teller (BET) method with N_2 (BEL SORP mini; Bel Japan Inc., Tokyo, Japan). The morphological features of the powder were observed using a transmission electron microscope (TEM, JEM-2010F; JEOL Ltd., Tokyo, Japan). The surface chemical composition and Mn valence were measured using XPS.

Activity measurements were conducted as described for our previous studies.^{7),12),13),16)} The solution of 2-naphthol ($\text{C}_{10}\text{H}_7\text{OH}$; Wako) was prepared by dissolving it into an acetonitrile ($\text{C}_2\text{H}_3\text{N}$; Wako)–water mixture (1:99 volume ratio) solvent (2-naphthol concentration: 4.0×10^{-5} mol/L). The MnO_x modified TiO_2 powder was dispersed into the solution heated at 50°C (by 0.2 g/100 mL). The suspension was stirred at 300 rpm with air bubbling by 120 mL/min. After filtration, the 2-naphthol concentration in the solution was analyzed from absorption at 223 nm, which is characteristic to 2-naphthol,²⁹⁾ using UV–vis absorption spectra obtained using a UV–vis scanning spectrophotometer (V-660; Jasco Corp., Tokyo, Japan).

Moreover, effects of the UV illumination or heat treatment on decomposition activity after repeated reactions in the dark were evaluated. The decomposition activity on 2-naphthol in water at 50°C was evaluated in the dark under the procedure described above. The sample was filtrated and dried at room temperature in vacuum for 24 h. Then the decomposition activity measurement in the dark was conducted again. After drying at room temperature, UV illumination (light intensity: 1.5 mW/m^2 at 380 nm) for 72 h or heat treatment at 80°C for 1 h in ambient air was conducted. After these treatments, activity measurements were conducted in the dark.

3. Results and discussion

3.1 Experiment using rutile single crystals

Figure 1 displays AFM images of rutile single crystals before MnO_x modification. Both (110) and (001) were smooth. The respective arithmetic surface roughness (R_a) values of these faces were 0.481 nm and 0.506 nm. **Figure 2** presents AFM images after MnO_x modification and Mn2p peaks obtained using XPS from the (110) and (001). The R_a values were increased to 1.79 nm [(110)] and 3.69 nm [(001)]. The coated film was porous, with thickness of approximately 20 nm. The thickness difference might result from the wettability difference against the ethanol solution of $\text{Mn}(\text{acac})_3$ used for coating. However, even under high magnification, observation of clear MnO_x cluster images was not feasible. Probably, its primary size is extremely small, as described in our previous study.¹³⁾

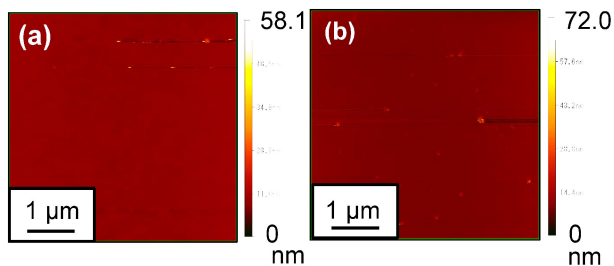


Fig. 1. AFM images of single crystal surface before MnO_x modification: (a) (110), and (b) (001).

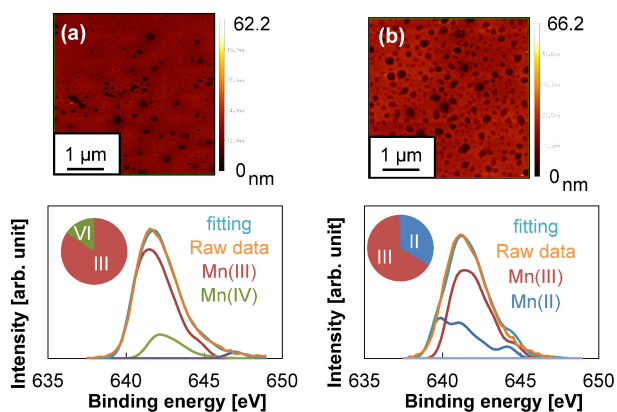


Fig. 2. AFM images of single crystal surface and XPS peak of $\text{Mn}_{2p_{3/2}}$ after MnO_x modification: (a) (110) and (b) (001).

Because of five-state degeneracy, the peak of $\text{Mn}_{2p_{3/2}}$ includes five major multiplet peaks with a satellite peak. We assumed Gaussian functions on these multiplet and satellite peaks, and prepared peaks of Mn(II), Mn(III), and Mn(IV) with fixing of the position and the height ratio among these multiplet and satellite peaks based on some earlier reports of the relevant literature.^{22),23)} Then the entire intensity of the obtained peaks of Mn(II), Mn(III) and Mn(IV), and full width at half maximum (FWHM) of the multiplet and satellite peak (this value was set constant for all peaks) were altered to fit the practical peaks of XPS. We used “solver” software of Excel (Microsoft Corp.) for this procedure. The final peak top energy and FWHM values are listed in *Supporting Information*. Because of the small concentration of Mn on the surface of TiO_2 powders by the CCC process (described below), the intensity of $\text{Mn}_{2p_{1/2}}$ is insufficient and the influence of background noise cannot be ignored. Therefore, we discussed the valence of Mn solely by the result of $\text{Mn}_{2p_{3/2}}$ in this study.

As shown in Fig. 2, analysis by XPS revealed that the major valences of Mn in (110) were Mn(IV) and Mn(III), whereas those in (001) were Mn(III) and Mn(II). This result implies that the valence of MnO_x cluster prepared by CCC processing depends on the crystal face, even though the base material is rutile. As described above, the high valence state of Mn reflects a large amount of oxidation capability against organic compounds. Results show that the rutile with a high (110) surface area ratio is advantageous for high decomposition activity.

Table 1. Results of energy calculation

	E [eV]
TiO_2 (110)	-118810
Mn_2O_2 on TiO_2	-125420
Mn_2O_3 on TiO_2	-125850
Mn_2O_4 on TiO_2	-126290

Photo-deposition method is well known to enable a prospective means of loading a noble metal or oxide nanoparticles onto the TiO_2 surface.^{30)–35)} Very recently, Huang et al.³⁵⁾ reported loading of MnO_x onto a TiO_2 surface via photo-assisted deposition. During the synthesis procedure, MnO_4^- was reduced and flocculent MnO_x in-situ anchored on TiO_2 . Therefore, we also tried to modify rutile single crystals with MnO_x using photo-deposition. The single crystals annealed at 600°C were soaked into a KMnO_4 (Wako) aqueous solution (1.0 g/L). Then UV illumination (UV intensity at the topmost sample surface: $10 \text{ mW}/\text{cm}^2$) was conducted for 1 h using a UV illuminator (LA-410UV-1; Hayashi Watch Works, Tokyo, Japan) equipped with a Hg–Xe lamp. The valence in MnO_x obtained from this process on (110) was Mn(II): 9.9%, Mn(III): 83.6%, and Mn(VI): 1.6%, and that on (001) was Mn(III): 70.1%, Mn(IV): 21.7%, Mn(VI): 1.7%, and Mn(VII): 6.5%. This result was different from that obtained by CCC processing, probably because (110) is a reduction dominant surface in rutile under UV illumination.¹⁹⁾

Recently, the structure and state of several transition metal oxide clusters such as SnO_x , PbO_x and CuO on (110) of rutile prepared by CCC processing were investigated using a computational approach.^{36),37)} After reviewing results of those studies, we conducted structural optimization and formation energy calculation for MnO_x clusters on (110) of rutile using software (Material Studio 8.0). We used the PBE GGA function, with calculations conducted under the following conditions: K-point mesh, $1 \times 1 \times 1$; 400 eV cutoff energy. Initially, structural optimization of rutile unit cells was done. Then (110) was cut with exposure of a dangling bond of oxygen. The structure was built until the fourth atomic layers. After preparing a super lattice by 3×4 , a vacuum slab (thickness: 1 nm) layer was set on the surface. Structural optimization was performed for the topmost two layers. The bottom two layers were fixed. After surface structure optimization, MnO_x cluster was set on the surface. After we reviewed some recent publications,^{36),37)} we set the same cluster for Mn_2O_4 as PbO_2 , for Mn_2O_3 as Fe_2O_3 , and for MnO as PbO and CuO on rutile (110). The initial models of MnO_x cluster on (110) of rutile are presented in *Supporting Information*. Then structure optimization was conducted again under the same condition. The results of formation energy calculations for each state are presented in **Table 1**. The energy order was $\text{Mn}_2\text{O}_2 > \text{Mn}_2\text{O}_3 > \text{Mn}_2\text{O}_4$, which means Mn_2O_4 is the most stable on (110) of rutile. This result, which corresponds to experimentally obtained results, provides one plausible explanation of the appearance of Mn(IV) and Mn(III) valence state on (110) of rutile.

Unfortunately, the surface structure of rutile (001) with transition metal oxide cluster has not been well investigated to date. Therefore, the energy calculation for (001) should be addressed in future work.

3.2 Preparation and activity of rutile nanorod powder

Figure 3 presents XRD patterns of powders obtained from hydrothermal processing. All samples were rutile single phase. The sample prepared at 200°C for 12 h exhibited the highest integrated intensity ratio of the XRD peaks between (110) and (002) (I_{110}/I_{002}). TEM micrographs of this sample and a commercial rutile powder are displayed in **Fig. 4**. The powder prepared at 200°C for 12 h was elongated to [001] and possessed rod-like morphology. Chen et al. provided an explanation for this trend from the viewpoint of ligand field by assuming a Ti(IV) complex ion such as $[Ti(OH)_nCl_m]^{2-}$ ($n + m = 6$).³⁸ We used these samples for MnO_x modification. The specific surface area after modification was $17 \text{ m}^2/\text{g}$, which was almost half the value of the sample prepared from a commercial rutile powder (approx. $37 \text{ m}^2/\text{g}$). Hereinafter, samples prepared from the nanorod powder and a commercial rutile powder are denoted, respectively, as NRs-Mn3 and TiO_2 -Mn3.

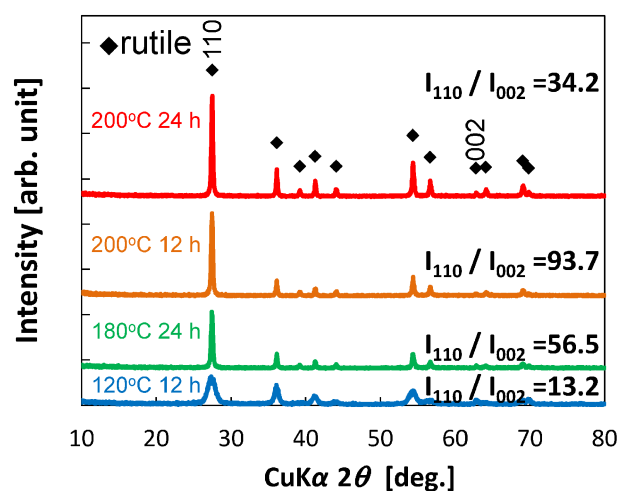


Fig. 3. XRD patterns of samples prepared using hydrothermal processing.

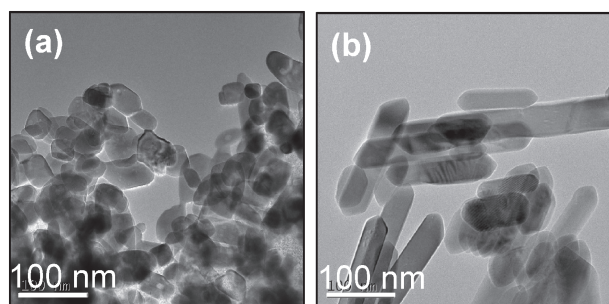


Fig. 4. TEM micrographs of rutile powders: (a) commercial rutile powder fired at 600°C, and (b) synthesized rutile powder synthesized hydrothermal processing under 200°C 12 h.

Figure 5 depicts the XPS peaks of $Mn2p_{3/2}$ in MnO_x on TiO_2 -Mn3 and NRs-Mn3. The valences of Mn in MnO_x for NRs-Mn3 were Mn(IV): 35.4% and Mn(III): 64.6%, this ratio is greater than that for TiO_2 -Mn3 [Mn(IV)/Mn(III) = 23.6/76.4]. This result is expected to be attributable to the area ratio difference between (110) and (001). However, the surface Mn concentration (atom %, Mn/Ti) of NRs-Mn3 (0.15) was lower than that of TiO_2 -Mn3 (0.23). Although the reason for this concentration difference remains unclear, surface wettability against the ethanol solution of $Mn(acac)_3$ might be different between the prepared nanorod rutile powder after hydrothermal treatment and the commercial rutile powder. The differences in peak top energy and FWHM values of peaks practically obtained by XPS were not significant, but we were unable to provide a detailed discussion of them in this report because background noise remains even for the $Mn2p_{3/2}$ peak, as presented in Fig. 5. Therefore, we conducted only valence separation of $Mn2p_{3/2}$ peak in this study.

Figure 6 shows the concentration change of 2-naphthol in the solution with TiO_2 -Mn3 or NRs-Mn3 under dark conditions. Apparently, their activity seems similar. **Table 2** presents characters and decomposition activity of TiO_2 -Mn3 and NRs-Mn3. Both decomposition and adsorption contribute to the concentration change in the

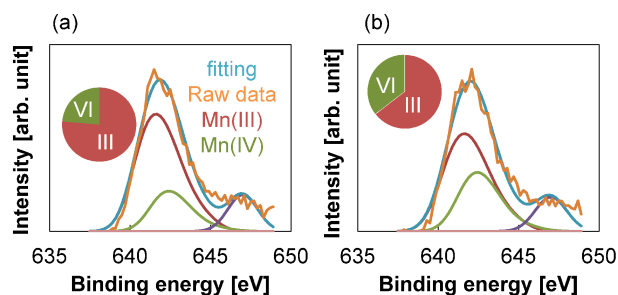


Fig. 5. XPS peak of $Mn2p_{3/2}$ in MnO_x on TiO_2 -Mn3 and NRs-Mn3: (a) TiO_2 -Mn3, and (b) NRs-Mn3.

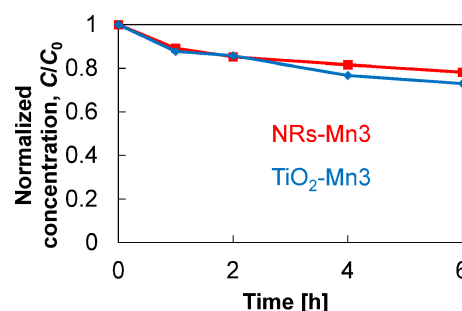


Fig. 6. Concentration change of 2-naphthol in the solution with TiO_2 -Mn3 or NRs-Mn3 under dark condition.

Table 2. Characters and decomposition activity of TiO_2 -Mn3 and NRs-Mn3

	Reaction constant [h ⁻¹]	Specific surface area [m ² /g]	Composition ratio (Mn/Ti)	Normalized Reaction constant [g/h·m ²]
TiO_2 -Mn3	0.039	37	0.23	0.0046
NRs-Mn3	0.025	16.5	0.15	0.010

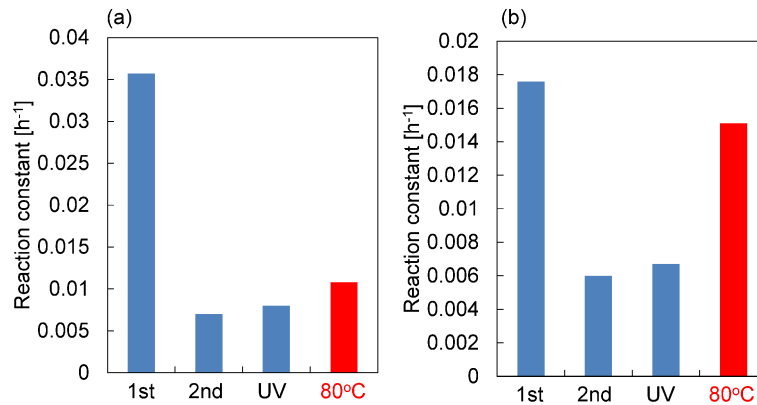


Fig. 7. Reaction constants for NRs-Mn3 and TiO₂-Mn3 in the concentration change of 2-naphthol in water at 50°C in the dark by repeated use, and that after UV illumination or heat treatment at 80°C.

early stage of the reaction time in this system. Therefore, we used concentration results from 1 to 6 h for calculation of the reaction constant for the decomposition activity. The values for NRs-Mn3 and TiO₂-Mn3 were, respectively, 0.025 and 0.039 h⁻¹. Those values correspond to those found in earlier previous studies.^{13),16)} The specific surface area and surface Mn concentrations differed. Therefore, we normalized the reaction constant by them. The value was 0.010 g/h·m² for NRs-Mn3, and 0.0046 g/h·m² for TiO₂-Mn3. The normalized activity for NRs-Mn3 was more than twice as much as that for TiO₂-Mn3. This result is also attributable to a high Mn(IV) ratio in MnO_x. Increasing the area ratio of (110) in rutile is an effective approach to increase the decomposition activity of this material in the dark.

Figure 7 presents reaction constants for TiO₂-Mn3 and NRs-Mn3 in the concentration change of 2-naphthol in water at 50°C in the dark through repeated use, and that after UV illumination or heat treatment at 80°C. Repeated use decreased the decomposition activity for NRs-Mn3 and TiO₂-Mn3. The sample batch for this experiment was different from that for Table 2, thus the reaction constant values for the 1st measurement in Fig. 7 were slightly different from those listed in Table 2. A similar trend was reported from our earlier study: it was attributed to the slow re-oxidation rate on the reduced MnO_x by dissolved oxygen during the MvK mechanism in water.^{13),16)} When UV light was illuminated onto the samples in the dark after using it twice, the decomposition activity recovered slightly. That recovery became remarkable when heat treatment was conducted at 80°C. These trends are the same for these two samples, but the effects of heat treatment are more remarkable for NRs-Mn3 than for TiO₂-Mn3. Reduced MnO_x on the reduction site of TiO₂ is difficult to re-oxidize by a photocatalytic reaction. Therefore, heat treatment is more effective than UV illumination. The difference in the effect of heat treatment between NRs-Mn3 and TiO₂-Mn3 might be attributable to the stability of Mn(IV) on (110) of rutile. Mn(IV) is stable on (110); moreover, the (110) area ratio against the entire surface for NRs-Mn3 is higher than that for TiO₂-Mn3. Therefore, heat treatment is more effective for NRs-Mn3

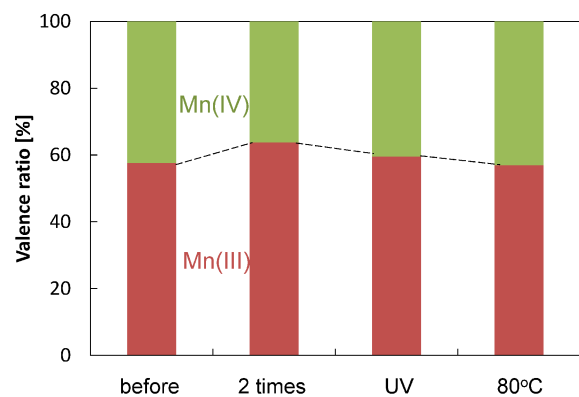


Fig. 8. Valence change of Mn in MnO_x on NRs-Mn3 at each process presented in Fig. 7.

than for TiO₂-Mn3. Figure 8 depicts the valence change of Mn in MnO_x on NRs-Mn3 at each process in Fig. 7. The valence change [Mn(IV) concentration change] of NRs-Mn3 correlated with decomposition activity. Similar correlation was confirmed also for TiO₂-Mn3.¹³⁾ It is noteworthy that the practical decomposition pathway of 2-naphthol in this system is a subject for future work, thereby quantitative analysis between the reduction amount of Mn and 2-naphthol concentration remains unclear at this stage. This work demonstrated that MvK mechanism of MnO_x depends strongly on the valence of Mn, and that appropriate design between MnO_x and the base material is an important factor for these materials with high decomposition activity.

4. Summary

In this study, MnO_x was modified onto single crystals and powders of rutile. Then the decomposition activity of the rutile samples on 2-naphthol in water was evaluated in the dark. The crystal face dependence of the activity was discussed. When MnO_x was modified onto (110) and (001) of the single crystals by CCC processing, Mn(IV) and Mn(III) states were dominant in (110), whereas Mn(III) and Mn(II) states were dominant in (001). However, in the case of photo-deposition processing, Mn(II) state appeared in (110), and Mn(IV) state appeared in (001), probably

because (110) is reduction dominant in rutile under UV illumination. The results of energy calculation provided a similar trend for Mn valence in MnO_x cluster on (110) by CCC processing. Based on this result, we prepared rutile nanorod powder with a high area ratio of (110) by hydrothermal technique. The sample from the nanorod (NRs–Mn3) possessed a higher Mn(IV) ratio than the sample from commercial rutile powder (TiO₂–Mn3) after MnO_x modification by CCC processing. The activity of NRs–Mn3 after normalization by specific surface area and Mn concentration was more than two times higher than that of TiO₂–Mn3. Although the activity of these samples in the dark decreased gradually through repeated use, it recovered by UV illumination at room temperature or heating at 80°C in ambient air. The degree of recovery by the heat treatment for NRs–Mn3 was more remarkable than that for TiO₂–Mn3.

Acknowledgements The authors are grateful to the staff of the Center of Advanced Materials Analysis (CAMA) at Tokyo Institute of Technology for various characterization and helpful discussion on this study. This work was supported in part by a Grant-in-Aid for Scientific Research from the Ministry of Education, Culture, Sports, Science, and Technology of Japan (16K14382).

References

- 1) A. Fujishima, X. Zhang and D. A. Tryk, *Surf. Sci. Rep.*, **63**, 515–582 (2008).
- 2) I. Rosenberg, J. R. Brock and A. Heller, *J. Phys. Chem.*, **96**, 3423–3428 (1992).
- 3) N. Takeda, T. Torimoto, S. Sampath, S. Kuwabara and H. Yoneyama, *J. Phys. Chem.*, **99**, 9986–9991 (1995).
- 4) M. R. Hoffmann, S. T. Martin, W. Choi and D. W. Bahnemann, *Chem. Rev.*, **95**, 69–96 (1995).
- 5) S.-Y. Lee and S.-J. Park, *J. Ind. Eng. Chem.*, **19**, 1761–1769 (2013).
- 6) K. Sunada, T. Watanabe and K. Hashimoto, *J. Photochem. Photobiol. A Chem.*, **156**, 227–233 (2003).
- 7) Q. Jin, H. Arimoto, M. Fujishima and H. Tada, *Catalysts*, **3**, 444–454 (2013).
- 8) J. Wang, R. Yunus, J. Li, P. Li, P. Zhang and J. Kim, *Appl. Surf. Sci.*, **357**, 787–794 (2015).
- 9) V. Iablokov, K. Frey, O. Geszti and N. Kruse, *Catal. Lett.*, **134**, 210–216 (2010).
- 10) H. Rahaman, R. M. Laha, D. K. Maiti and S. K. Ghosh, *RSC Adv.*, **5**, 33923–33929 (2015).
- 11) J. Wang, R. Yunus, J. Li, P. Li, P. Zhang and J. Kim, *Appl. Surf. Sci.*, **357**, 787–794 (2015).
- 12) H. Tada, Q. Jin, H. Nishijima, H. Yamamoto, M. Fujishima, S. Okuoka, T. Hattori, Y. Sumida and H. Kobayashi, *Angew. Chem. Int. Edit.*, **50**, 3501–3505 (2011).
- 13) M. Shiohara, T. Isobe, S. Matsushita and A. Nakajima, *Mater. Chem. Phys.*, **183**, 37–43 (2016).
- 14) T. Zhang, D. Wang, Z. Gao, K. Zhao, Y. Gu, Y. Zhang and D. He, *RSC Adv.*, **6**, 70261–70270 (2016).
- 15) “Structure and Properties of Inorganic Solids” ed. F. S. Galasso, Pergamon Press Ltd., Oxford, translated by M. Kato and K. Uematsu to “Fain seramikusu no kesshou kagaku”, Agune-Press, Tokyo (1984) p. 53 [in Japanese].
- 16) D. Tanaka, T. Isobe, S. Matsushita and A. Nakajima, *J. Ceram. Soc. Jpn.*, **126**, 122–127 (2018).
- 17) R. Wang, N. Sakai, A. Fujishima, T. Watanabe and K. Hashimoto, *J. Phys. Chem. B*, **103**, 2188–2194 (1999).
- 18) A. Nakajima, S. Koizumi, T. Watanabe and K. Hashimoto, *J. Photochem. Photobiol. A*, **146**, 129–131 (2001).
- 19) T. Ohno, K. Sarukawa and M. Matsumura, *New J. Chem.*, **26**, 1167–1170 (2002).
- 20) P. A. Morris Hotsenpiller, J. D. Bolt, W. E. Farneth, J. B. Lowekamp and G. S. Rohrer, *J. Phys. Chem. B*, **102**, 3216–3226 (1998).
- 21) J. B. Lowekamp, G. S. Rohrer, P. A. Morris Hotsenpiller, J. D. Bolt and W. E. Farneth, *J. Phys. Chem. B*, **102**, 7323–7327 (1998).
- 22) H. W. Nesbitt and D. Banerjee, *Am. Mineral.*, **83**, 305–315 (1998).
- 23) M. C. Biesinger, B. P. Payne, A. P. Grosvenor, L. W. M. Lau, A. R. Gerson and R. S. C. Smart, *Appl. Surf. Sci.*, **257**, 2717–2730 (2011).
- 24) Q. Wu, J. Xu, Q. Zhuang and S. Sun, *Solid State Ionics*, **177**, 1483–1488 (2006).
- 25) F. Larachi, J. Pierre, A. Adnot and A. Bernis, *Appl. Surf. Sci.*, **195**, 236–250 (2002).
- 26) Z. Wang, G. Shen, J. Li, H. Liu, Q. Wang and Y. Chen, *Appl. Catal. B-Environ.*, **138–139**, 253–259 (2013).
- 27) Q. Zhang and L. Gao, *Langmuir*, **19**, 967–971 (2003).
- 28) K. Yasui, T. Isobe and A. Nakajima, *Mater. Lett.*, **64**, 2036–2039 (2010).
- 29) L. Guru Prasad, V. Krishnakumar, G. Shanmugam and R. Nagalakshmi, *Cryst. Res. Technol.*, **45**, 1057–1063 (2010).
- 30) F. Zhang, N. Guan, Y. Li, X. Zhang, J. Chen and H. Zeng, *Langmuir*, **19**, 8230–8234 (2003).
- 31) B. Xi, X. Chu, J. Hu, C. S. Bhatia, A. J. Danner and H. Yang, *Appl. Surf. Sci.*, **311**, 582–592 (2014).
- 32) W. Yi, C. Yan, M. S. Hamdy, J. Baltrusaitis and G. Mul, *Appl. Catal. B-Environ.*, **154–155**, 153–160 (2014).
- 33) A. Tanaka, K. Hashimoto and H. Kominami, *Chem. Commun.*, **47**, 10446–10448 (2011).
- 34) E. S. Baeissa, *J. Ind. Eng. Chem.*, **20**, 3761–3766 (2014).
- 35) L. Huang, X. Hu, S. Yuan, H. Li, T. Yan, L. Shi and D. Zhang, *Appl. Catal. B-Environ.*, **203**, 778–788 (2017).
- 36) M. Nolan, A. Iwaszuk, A. K. Lucid, J. J. Carey and M. Fronzi, *Adv. Mater.*, **28**, 5425–5446 (2016).
- 37) A. Iwaszuk and M. Nolan, *J. Mater. Chem. A*, **1**, 6670–6677 (2013).
- 38) H. Cheng, J. Ma, Z. Zhao and L. Qi, *Chem. Mater.*, **7**, 663–671 (1995).